REFLEX-TRIODE GEOMETRY OF THE VIRTUAL CATHODE OSCILLATOR

by

MATTHEW B. LARA, B.S.E.E.

A THESIS

IN

ELECTRICAL ENGINEERING

Submitted to the Graduate Faculty
of Texas Tech University
in Partial Fulfillment of the Requirements
for the Degree of

MASTER OF SCIENCE

IN

ELECTRICAL ENGINEERING

Approved

December, 2003

ACKNOWLEDGEMENTS

I would like to express my graditude to Dr. Magne Kristiansen and Dr. Hermann Krompholz for initially giving me the opportunity to work in the lab as an undergraduate. I also would like to thank my committee members Dr. James Dickens, and Dr. John Mankowski for their input, and for saving me from the Spire 6000 by letting me construct my own pulser from the ground up.

This work would not have been possible without the help I received from Dino Castro, Lonnie Stevenson, Chris Hatfield, and Danny Garcia, who helped to teach me the art of machining and fabrication, and who helped to carry the burden of the mess associated with transformer oil.

Finally, thank you to the friends who are my family, and the family who are my friends for giving me support in my attempts to do everything at once.

TABLE OF CONTENTS

ABSTRACT

An eight-stage four-hundred kilovolt Marx generator, in connection with a 60 nanosecond pulse-forming line, is constructed and utilized as a pulsed source to power a triode version of the Virtual Cathode Oscillator (Vircator). Eight .1uF capacitors, charged to 50kV each, are switched in series by dry-air pressurized spark gaps. The energy from the bank charges a 23 ohm oil transmission line, breaking a peaking gap when the maximum voltage is reached, delivering a 60 ns-400kV pulse to the diode. The design of the "Reflex-Triode" geometry Vircator is based upon claims of high efficiency by Didenko et al.[1] A previously constructed TTU Vircator includes a unique E-beam source, the "brush" cathode; in which a circular array of pins is used as an explosive field emission source to produce relatively high beam currents. The anode consists of a round wire mesh through which the E-beam passes, generating a dense cloud of negative charge known as a "Virtual Cathode." This initial phase of testing is composed of basic operation of the entire system and baseline output power and efficiency measurements.

LIST OF FIGURES

CHAPTER I

INTRODUCTION

The use of the Virtual cathode oscillator as a pulsed, high-power microwave source has been of extreme interest to the Pulsed-Power community for almost twenty years. The relative mechanical simplicity, robustness of design, and no required external magnetic-field, make it an ideal candidate for practical EMP applications. In particular, the planar geometry offers a low-cost, minimal design with a controversial history of low to moderate efficiencies [1].

Using a 1kJ peak output Marx generator in connection with a 60ns pulse-forming line, and a previously constructed TTU Vircator, these numbers are either refuted or substantiated using a number of different cathode designs. Calibrated B-dot probes and baluns are used in the far field to obtain reliable power and frequency information for the system.

CHAPTER II

EXPERIMENTAL CONFIGURATION

2.1 Marx Generator

To generate an electron-beam current high enough to not be space-charge limited (tens of kiloamps), a voltage of 400-500kV is needed (400kV at the 20 Ohm diode impedance yields 20kA). To achieve multi-hundred kilovolt output, an eight-stage Marx Generator is employed due to its relatively simple construction, and availability of materials.[2] One kilo-joule is chosen for the desired output of the Marx yielding a total bank capacitance of:

$$E_{MARX} = \frac{1}{2} C_{MARX} V_{MARX}^{2}$$

where,

E_{MARX} = total energy of Marx Bank

V_{MARX} = total output voltage of Marx Bank

C_{MARX} = total capacitance of erected Marx

$$C_{MARX} = 2 \frac{1kJ}{(400kV)^{2}} = 1.25 \times 10^{-8} F$$

Eight *Maxwell 31885* 100nF capacitors are used because of their availability, physical dimensions, and high voltage rating of 75kV. For the before mentioned usage, the capacitors are only charged, at a maximum to 75% of their rated voltage (50kV), yielding a maximum output of 400kV for the system.

The principle of the Marx generator requires that with the triggering of the first gap(s), the successive are either over-voltaged, or triggered by the seeding of photons from UV light produced by previous gaps. However, the geometry/arrangement of the capacitors and gaps does not allow the latter, and so the former must be assured. To properly over-voltage each stage, some manner of interstage capacitance is used. This allows for each stage to only see its D.C. charge (40-50kV), until the first gap is triggered, at which point it experiences an electric-field higher than the breakdown field for the gap. Each successive stage is triggered by the previous gap in this fashion. Traditionally, a stray capacitance is employed between each stage to achieve inter-stage coupling. For the TTU system this interstage, or "forward-feeding" capacitance is achieved by the addition of extra bulk to the capacitor-to-gap connections (Figure 2.1.). This extra conductor material comes off the bank as sixteen 1" by 4" copper tabs facing the ground plane, so as to develop capacitance between ground and each stage. The rule of thumb for good forward-feeding is an inter-stage capacitance that is at least ten times the gap capacitance; a condition easily achieved with a gap capacitance of only several picofarads [3].

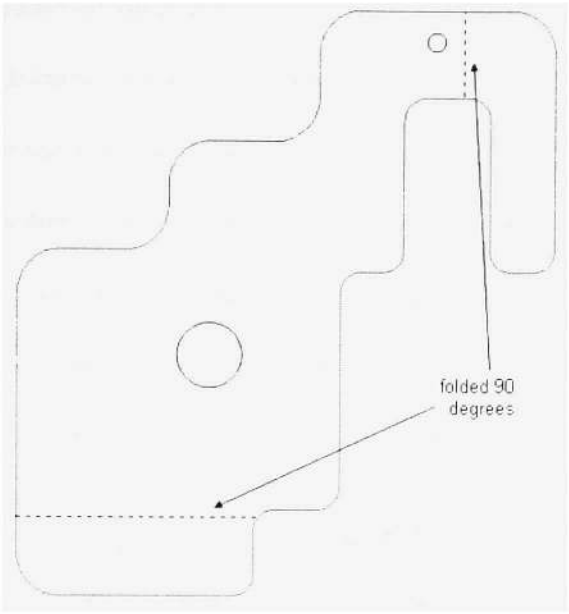

Figure 2.1. Cap-to-gap connector

Parallel charging of the Marx generator requires high-voltage resistors between each stage. The value of each resistor is determined by the charging time of the bank, and an impedance high enough that the resistors look "open" when the bank is erected, therefore allowing the capacitor voltages to add in series. Because of the fact that bulk material resistors (carbon, wire-wound,etc..) do not allow good voltage handling at the physical dimensions required by the size of the system (i.e., each resistor must be appx. 5 inches long), water/copper-sulfate resistors are used. To obtain the proper value (5-10kiloOhms) for each resistor, one single resistor is partially constructed using a ¾ inch copper electrode clamped into the end of a 1 inch O.D., ¾ I.D., oil-resistant vinyl tube. An initial mixture of water and copper-sulfate is made based upon existing curves for the pulsed case [4]. The mixture is then poured into the tubing, and a second electrode is

placed (but not clamped) into the other end of the tubing. The resistor is tested with a high-voltage supply and a known value metering-resistor. From this, a divider ratio is determined, returning the value for the water resistor. This process is repeated with different copper-sulfate/water concentrations until a proper resistance is obtained. Once the correct solute-solvent ratio is determined, a one liter batch is made, and all sixteen charging resistors are constructed (one spare). Figure 2.2. shows the arrangement of the capacitors, switches, and resistors forming the Marx generator.

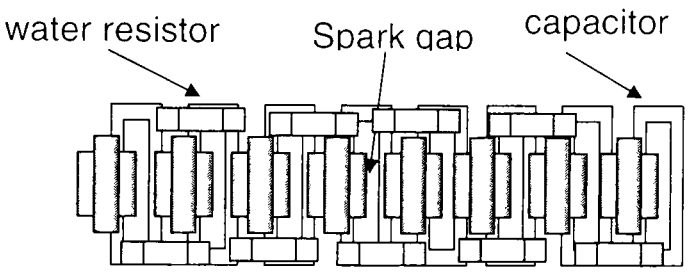

Figure 2.2. Arrangement of spark gaps, capacitors, and water resistors

Initially, the first gap was triggered with a 40kV pulse-pack and trigger generator applied to a third electrode. It was found that when charged, the gap electrodes were breaking to the very field-enhanced third electrode, triggering the gap before the bank could be fully charged. In response to this problem, a separate pressure dump was added to the first stage, allowing for a momentary switch connected to the purge solenoid of the first gap to control firing of the bank. When this switch is depressed, pressure quickly drops in the first gap, lowering the voltage hold-off, and subsequently breaking down the switch.

Due to inconsistencies in the triggering of the system, several adaptations were made to assure reliable usage of the machine. The first assumption made was a lack of capacitive coupling between the first couple of stages. In an attempt to rectify this issue, two high-voltage "doorknob" capacitors were attached in series across the first and second stages of the bank. Although this did at first aid in the over-voltaging of the first stages, the capacitors could not handle the sudden voltages stresses caused when the bank erected (see Figure 2.3.).

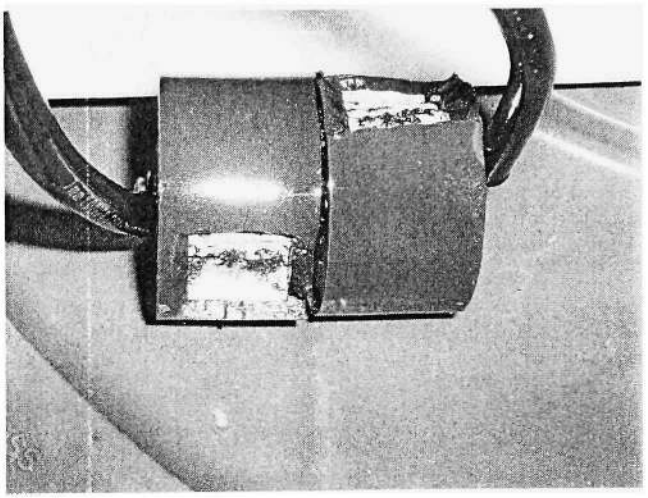

Figure 2.3. "Doorknob" capacitor failure

Connecting the first two gaps to the same pressure dump was the second, and successful method [5]. It should be noted that compressed air from the Physical Plant circulated through a desiccant chamber, was used as the supply pressure for the gaps, giving inconsistent firing only on certain days (probably due to small amounts of remaining moisture). However, when connected to separate dry Nitrogen cylinders, the generator gave consistent operation on an everyday basis. Figure 2.4. displays a plot of

the erected Marx generator voltage output recorded by the 1200:1 resistive divider. The signal is seen rising to 300kV (42kV charging), and then somewhat sporadically oscillating due to stray L and C values for the probe, reflections, and noise.

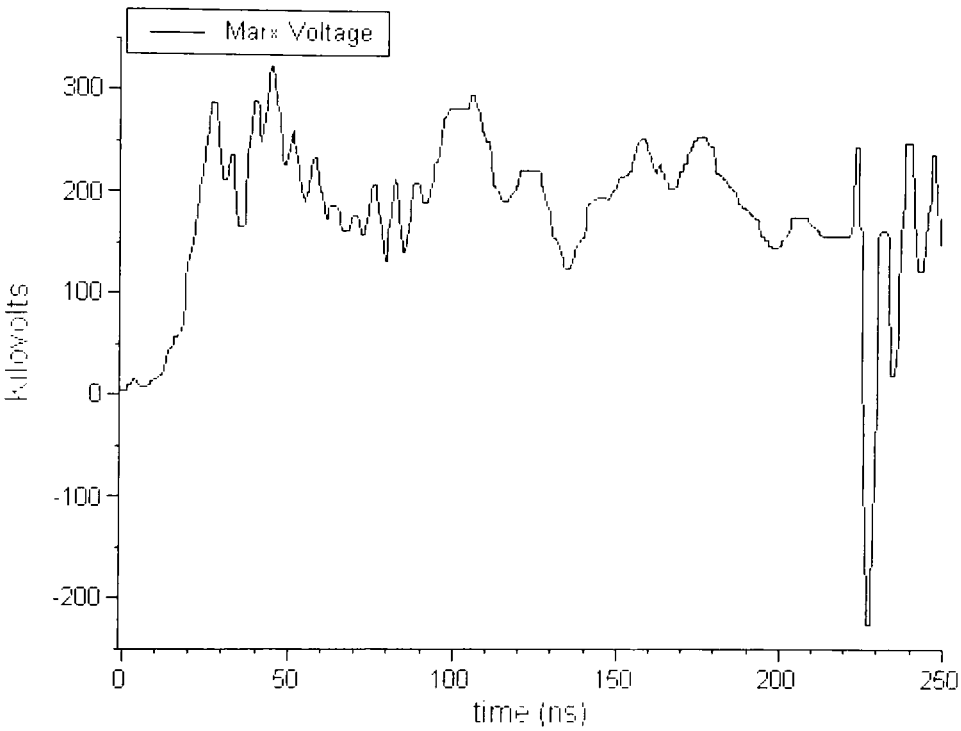

Figure 2.4 Marx Generator Voltage output

2.2 Pulse-Forming

Previous Vircator research has shown that a plasma channel can result in A-K gap closure and subsequent loss of microwave power, if the pulse is not relatively short (50-100ns) with a relatively fast risetime [6]. Due to stray inductance and lack of pulse-forming (as the Marx generator is simply one large capacitor when erected), a pulse-forming line (PFL) is required.

Design considerations for the PFL include a 15-20 Ohm characteristic impedance (to be matched with the diode), a two-way transit time of 50-100ns, and a voltage hold-off of up to 800kV (voltage doubling is assumed).

The first consideration, pulse length, establishes a physical length for the transmission line allowing impedance values to be calculated. A two-way transit time of 60ns is chosen because it lies between the previously selected range of 50-100ns, and is comparable to the pulse length used for the TTU coaxial Vircator.[5] From these criteria an approximate physical length of 6 meters (20 ft) is determined. Using this value in conjunction with known diameters for commercially available aluminum and copper tubing (outer and inner conductor respectively), values for the total inductance, capacitance, impedance, and Energy storage are found [8].

$$\tau_{ow} = \frac{l_{tline} \cdot \sqrt{\varepsilon_r}}{c}$$ one way transit time

$\tau_{ow} := 30 \cdot ns$

$\varepsilon_o := \frac{1}{36\pi} \cdot 10^{-9} \cdot \frac{F}{m}$

$\varepsilon_r := 2.2$ dielectric constant for transformer oil

$c := 3 \cdot 10^{8} \cdot \frac{m}{s}$

$l_{tline} := \tau_{ow} \cdot \frac{c}{\sqrt{\varepsilon_r}}$ length of transmission line

$l_{tline} = 6.068\,m$

$\mu := 4 \cdot \pi \cdot 10^{-7} \cdot \frac{H}{m}$

$b := \frac{7.70\,in}{2}$ outer conductor radius

$a := \frac{4.375\,in}{2}$ inner conductor radius

$L_{tline} := \frac{\mu}{2 \cdot \pi} \cdot \ln\left(\frac{b}{a}\right) \cdot l_{tline}$ total Inductance of transmission line

$L_{tline} = 6.86 \times 10^{-7}\,H$

$$C_{tline} := \frac{2 \cdot \pi \cdot \varepsilon}{\ln\left(\frac{b}{a}\right)} \cdot l_{tline}$$

total capacitance of transmssion line

$$C_{tline} = 1.312 \times 10^{-9}\,F$$

$$Z_{tline} := \sqrt{\frac{L_{tline}}{C_{tline}}}$$

total Impedance of transmission line

$$Z_{tline} = 22.868\Omega$$

$$V_{marx} := 400\,kV$$

$$E_{PFL} := \frac{1}{2} \cdot C_{tline} \cdot V_{marx}^{2}$$

total storage of transmission line

$$E_{PFL} = 104.95J$$

The construction details of the transmission line are as follows. A 24-foot section of 4" diameter copper tubing was purchased and cut to length for use as the center conductor. A conical brass insert was constructed to transition the line down to 1" while still being able to support the end of the copper tube (Figure 2.5.). The peaking gap side of the center conductor uses a similar copper insert to directly transition to the 1" copper-tungsten electrode (Figure 2.6.). The center of the copper tube is kept from sagging by using a piece of nylon all-thread threaded into the middle of the line, and then supported with a nut from the cap of the outer port (Figure 2.7). Ports were also placed at each end of the transmission line for diagnostics and removal of trapped air.

At first, insulating feed-throughs supported each end of the center conductor. These served the purpose of sealing the transmission line on both ends so that each component of the system could be serviced without having to drain all of the oil. However, after the first 100 shots the peaking gap feed-through failed due to trapped air in the o-ring groove, and the Marx-side feed-through failed several hundred shots later due to similar reasons (Figure 2.8.). Both were replaced with insulating supports without seals.

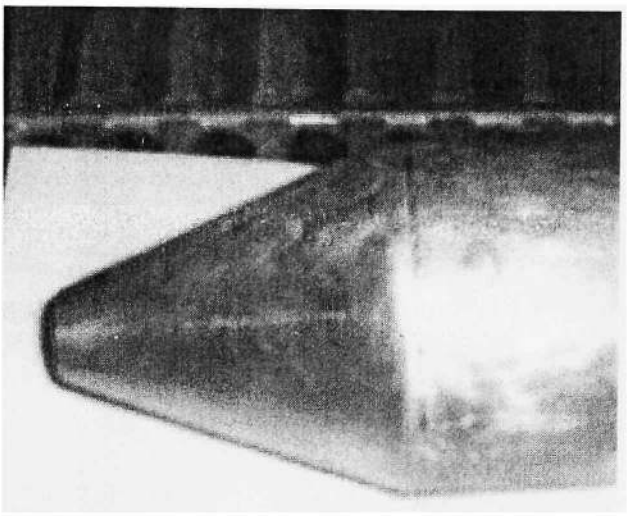

Figure 2.5. 4" to 1" transition

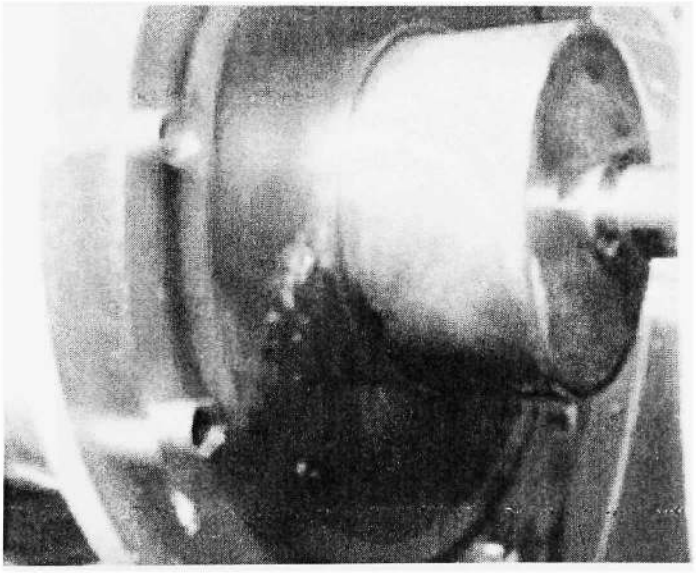

Figure 2.6. Peaking gap feed through w/ tracking

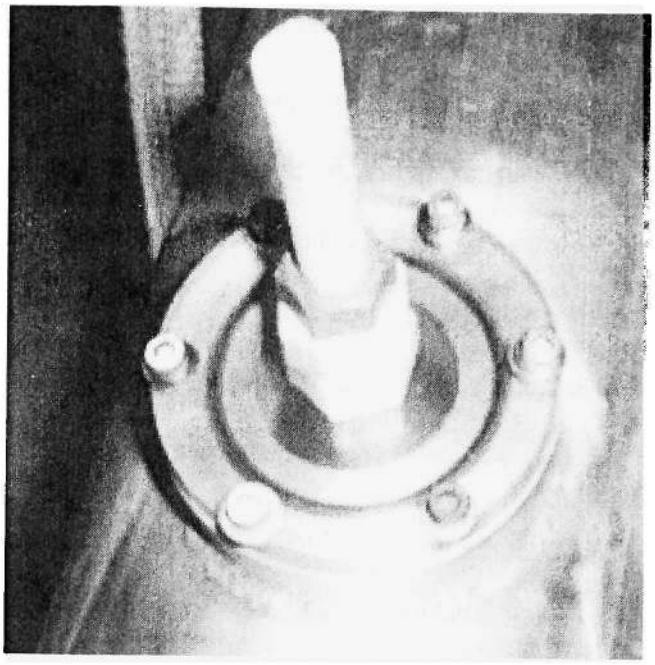

Figure 2.7 Center conductor support and port example

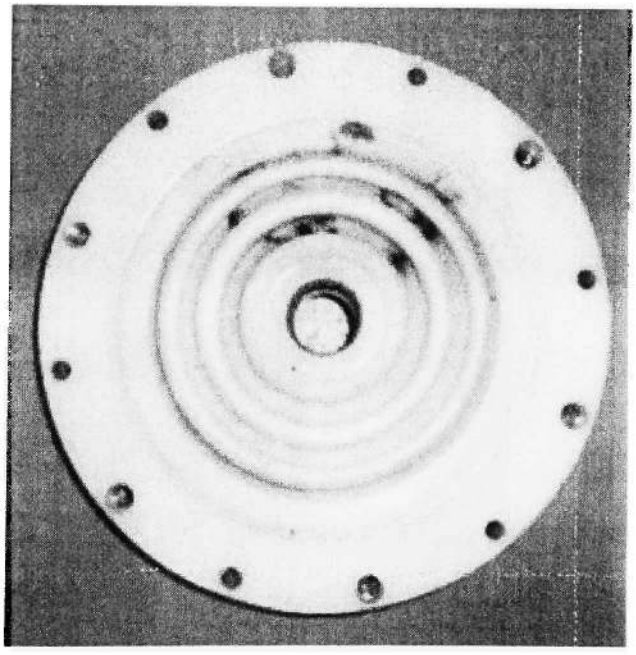

Figure 2.8 Marx -side feed-through with tracking

The transmission-line is terminated in a peaking gap constructed of two 1-inch copper-tungsten electrodes contained in a separate section of 8" Aluminum tube. The gap housing includes ports for filling/draining the oil, and diagnostics. It was initially thought that a pre-pulse resistor would be necessary to keep the load side of the gap from floating. An attempt was made at constructing a voltage-divider/pre-pulse resistor that could fit inside the 8" housing. Although such a device was constructed and tested, it later was removed because of failure, and lack of need (Figure 2.9.).

The gap distance was determined by first firing with a small gap spacing and opening the electrodes based upon the voltage waveforms in Figure 2.12. The plot shows the ideal case, in which the transmission line charges to its maximum at which point the switch closes, releasing the 60 ns of stored energy in the line. A "dummy" load was constructed for the initial testing of the switch. It consists of a 5-ohm carbon resistor in a coaxial configuration (Figure 2.10.).

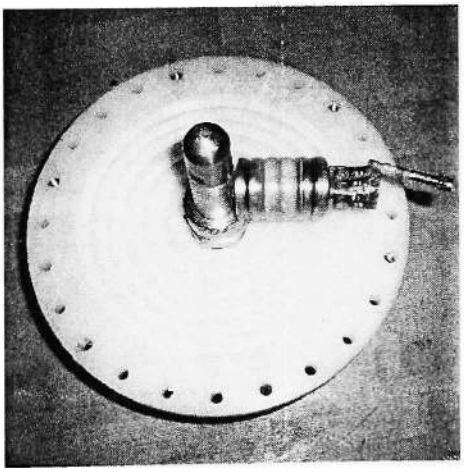

Figure 2.9. Vacuum feed-through, electrode, and pre-pulse/resistive divider

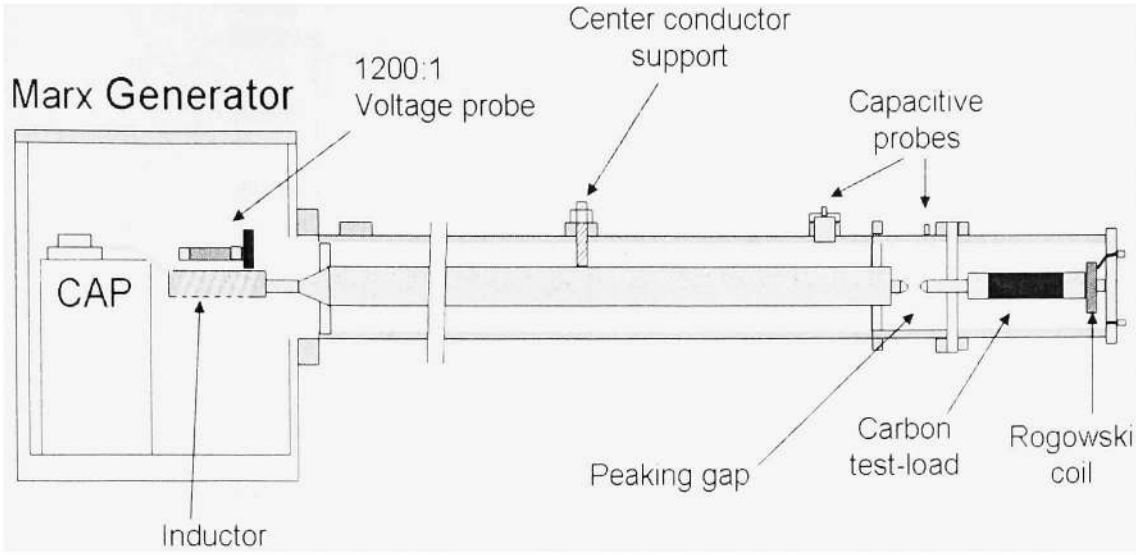

Figure 2.10a. Test Setup (with test load)

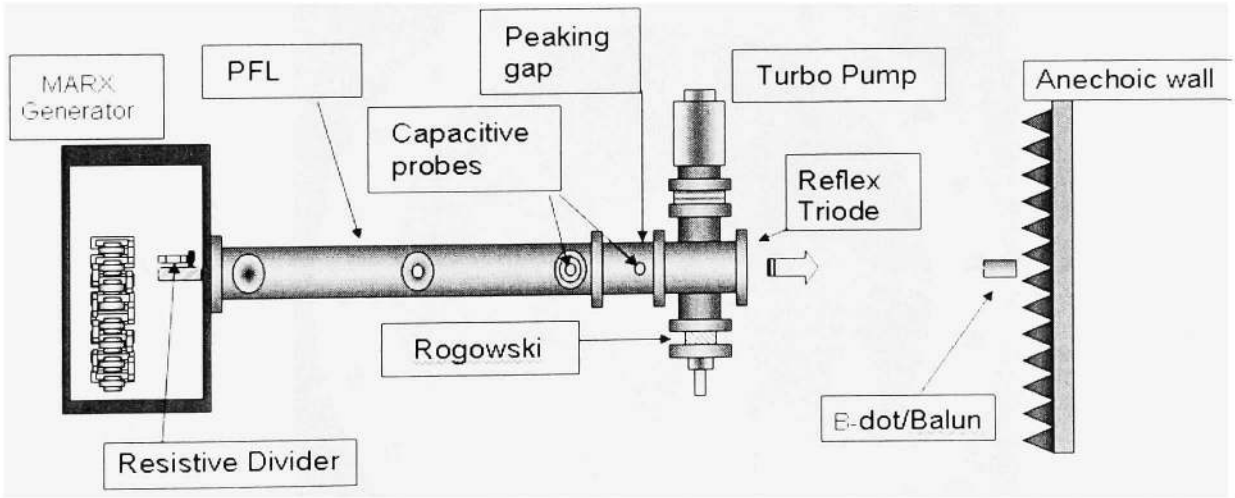

Figure 2.10b. Test setup (with Trriode)

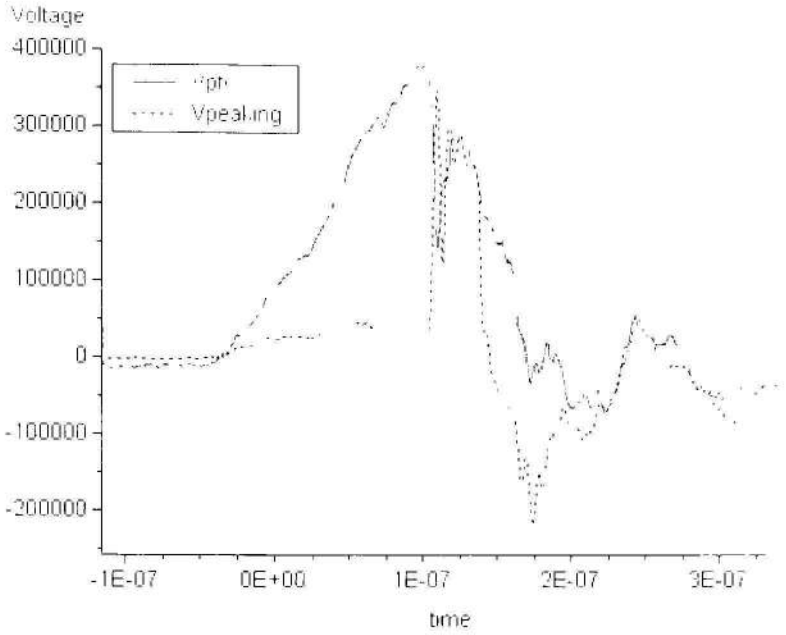

Figure 2.11. Transmission line and peaking gap voltage

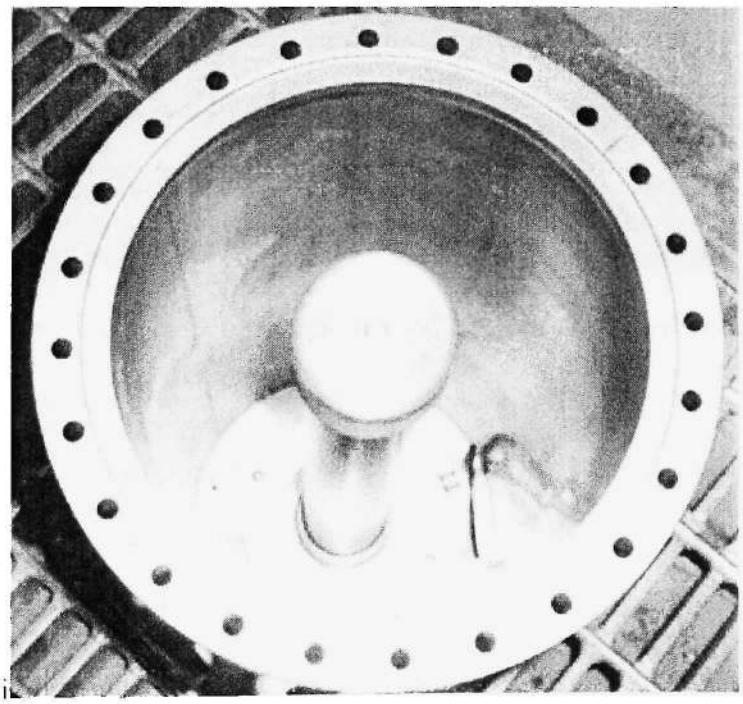

Figure 2.12. Test load with Rogowski coil

2.3 Diagnostics

In order to establish a baseline idea of efficiency for the vircator, input and output power for the system must be known. This data is collected using a set of capacitive and resistive voltage probes, high-speed current transformers, and B-dot RF detectors.

Starting from the Marx generator and working out toward the load, the first probe is a 1200:1 resistive divider. This probe is constructed of a 500 Ohm copper-sulfate water resistor and a "hockey-puck" style .5 Ohm carbon resistor (Figure 2.11.). The divider gives an idea of the Marx voltage as a comparison for the other voltage probes.

The next probe is a capacitive voltage divider placed into the last port on the transmission line (Figure 2.11.). The probe has a self-capacitance of ~400pF, which in conjunction with the capacitance developed between the exposed probe area and the inner conductor of the PFL, gives a voltage division ratio of 40,000:1.

The last of the voltage probes, located on the load side of the peaking gap, is also capacitively coupled. Voltage division is accomplished in the same manner as the previous detector. A 1" by 1" patch of Kepton tape is placed on the inner surface of the peaking gap chamber. The center conductor of a BNC feed-through pierces the tape and is soldered to a square section of copper tape inset on the Kepton. The capacitance of the probe is approximately 200pF, requiring a series resistance of 1Kohm to obtain the time constant necessary to resolve the 60ns waveform.

D.C charging of the PFL is used to calibrate the capacitive dividers. The slow charging time causes the gap to break at a much lower voltage than it would with the

Marx generator. Typically the switch broke at 45-50kV, giving 50-60mV of signal to the scope, and therefore yielding a sensitivity of 18,000:1 for the load-side probe.

Figure 12. shows a plot of the PFL and load voltages. The transmission line can be seen charging in 150 ns to 400kV (50 kV charge) at which point the switch closes, delivering 60 ns of stored energy to the load.

A Rogowski current transformer is used to obtain current measurements for the diode. A pre-calibrated Pearson coil could not be used for the system due to peak current and rise-time limitations. However, the Pearson coil was used for comparison to calibrate the Rogowski, showing it to have a sensitivity of ~.2V/A.

The beam current, typically around 10kA, gives a reasonable idea of the functioning of the Diode. i.e. if there is a high beam current with low microwave power in comparison to other shots, the B-dots and/or baluns are checked to make sure they are functioning properly.

To further understand the electron beam generated by the brush cathode, a piece of acetate film is placed over the anode screen. When subjected to the beam current, the film clouds over in a localized fashion allowing a visual diagnostic for determining where, and to what degree the brush is emitting (Figure 3.2.).

CHAPTER III

DATA

3.1 Pulser Data

Waveforms from the month of May offer a wide collection of complete data on the functioning and "tuning" of the pulser, with some qualitative comparison of microwave output, and no frequency comparison. The most complete set was taken in June and consists of material pertaining to input power, output power, and frequency. This set is only limited by the small number of shots taken, and the fact that some of the RF data clipped on the scope. The latter point is very important, as it gives insight to the adaptations used to extract both frequency and output power from the clipped sets. A discussion of this will be made along with the corresponding waveforms.

The final set of shots was taken during the first two weeks of October, at which point the machine required repairs beyond the timeline of the thesis. The October data is utilized for the information it gives on the affect of varied anode-cathode spacing.

It was hoped that a section dedicated to the operation of the Triode with the addition of a resonant cavity would be included, but due to the before mentioned failure only a brief section is dedicated to the cavity in Section 4 pertaining to future research suggestions.

All voltage, current and balun data was taken on the *Infinium* 500 Mhz digital oscilloscope. Figure 3.1. shows the scope data for a typical shot. The scope is triggered off of the peaking gap channel, and therefore shows the origin of the x-axis to be ~20ns

into the charging of the PFL. The waveforms pictured is an example of a "good" shot for the system. *i.e.* the PFL charges, and the peaking gap breaks at the maximum charging voltage for the line. From this, a strong beam current is generated, and consequentially, a strong microwave signal. Figure 3.2. is a scanned image of a piece of Acetate film that was placed on top of the Anode screen for several consecutive shots. The clouded areas occur where the beam was the strongest. Multiple points can be seen on the film indicating some emission from each nail on the cathode. The large clouded area on the periphery of the image is thought to be break-down that occurred from the cathode to the inner edge of the anode screen holder.

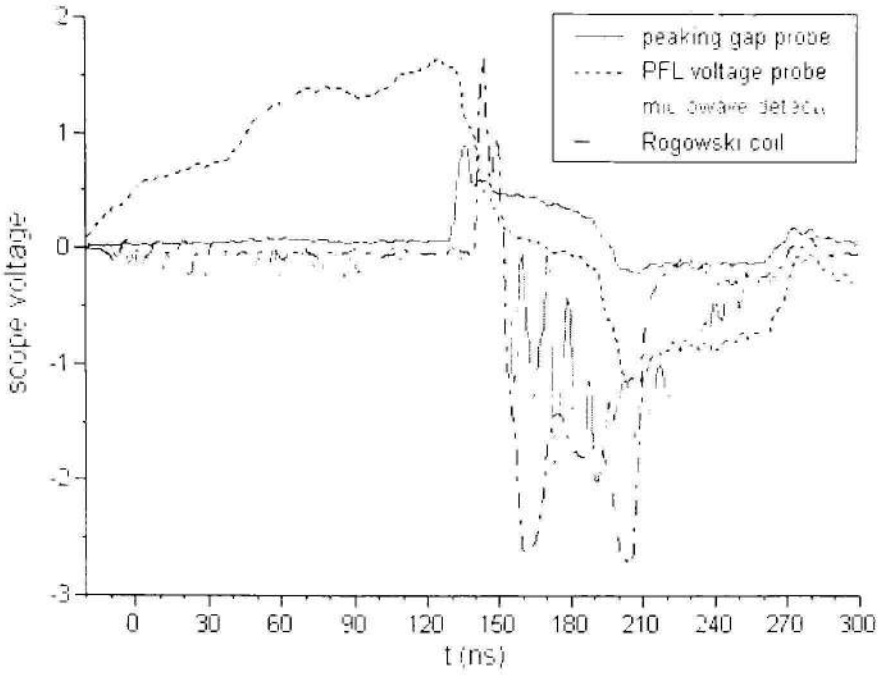

Figure .31. Typical raw scope data for the pulser

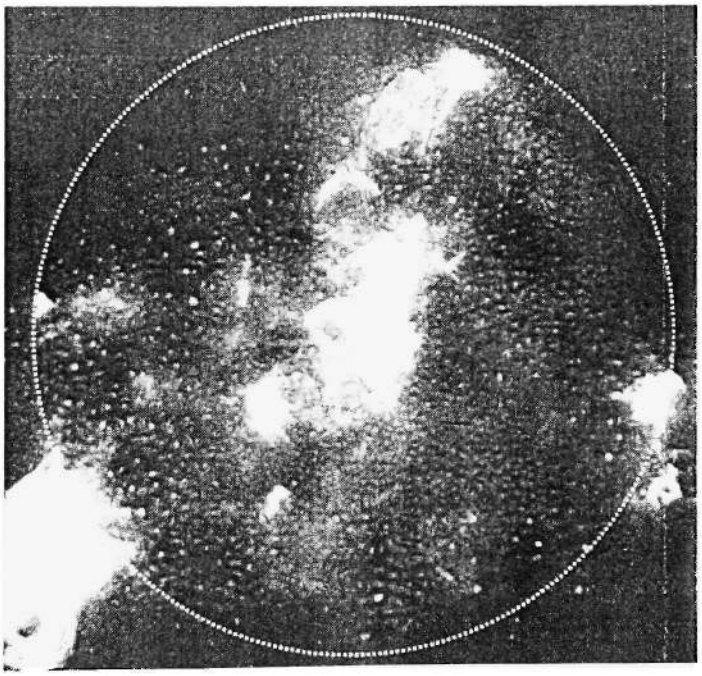

Figure 3.2. Scanned image of Acetate film showing cathode emission pattern

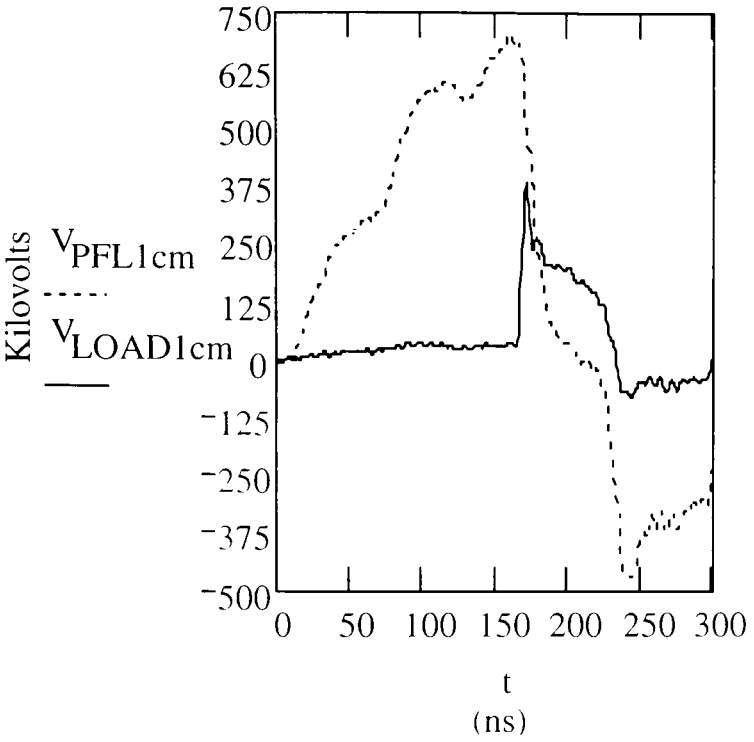

Figure 3.3. PFL and load voltages for 1cm A-K spacing

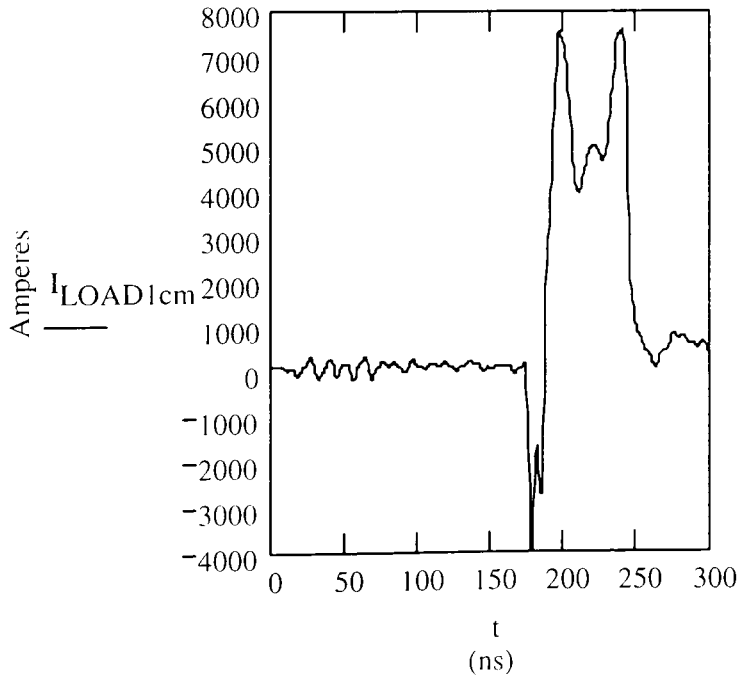

Figure 3.4. Beam current for 1cm A-K spacing

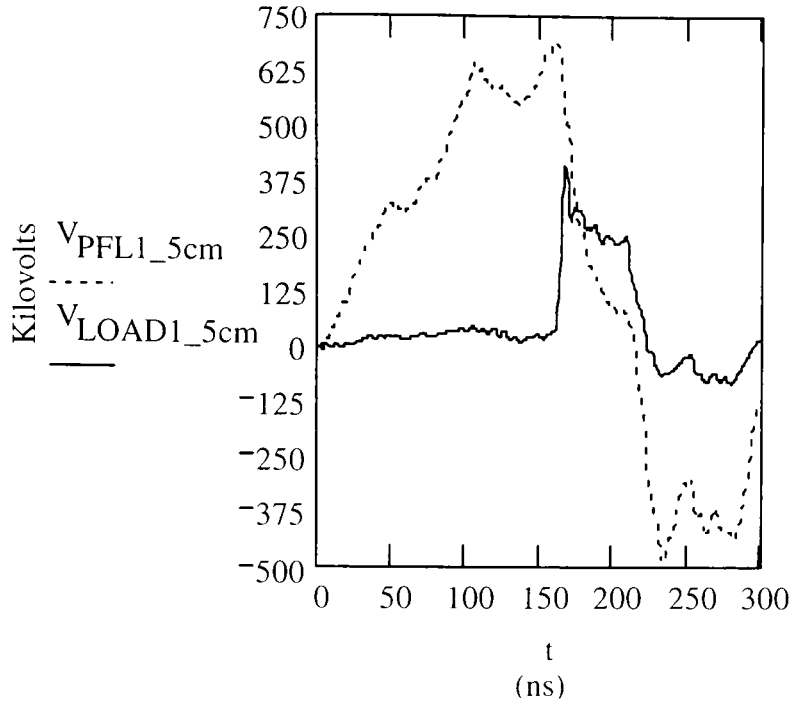

Figure 3.5. PFL and Load voltage for 1.5cm A-K spacing

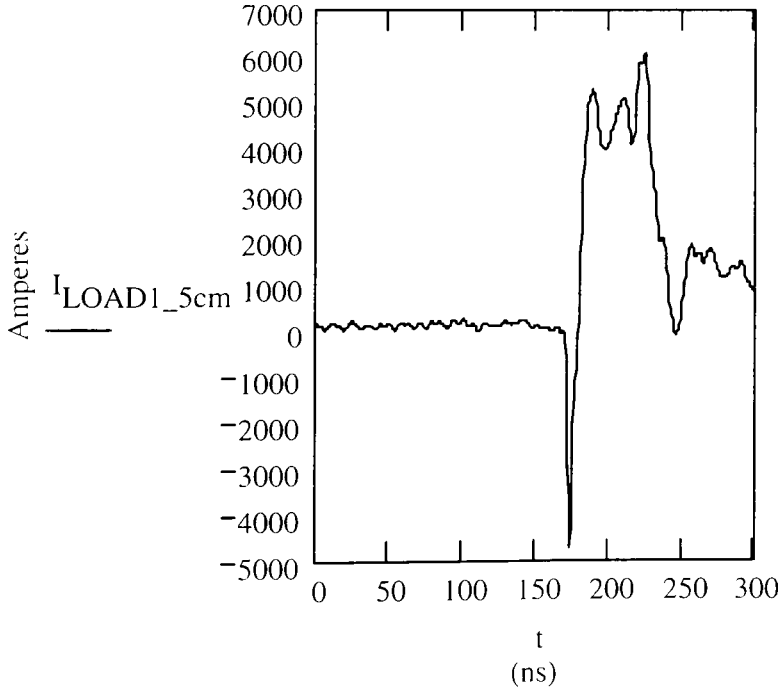

Figure 3.6. Beam current for 1.5 cm A-K spacing

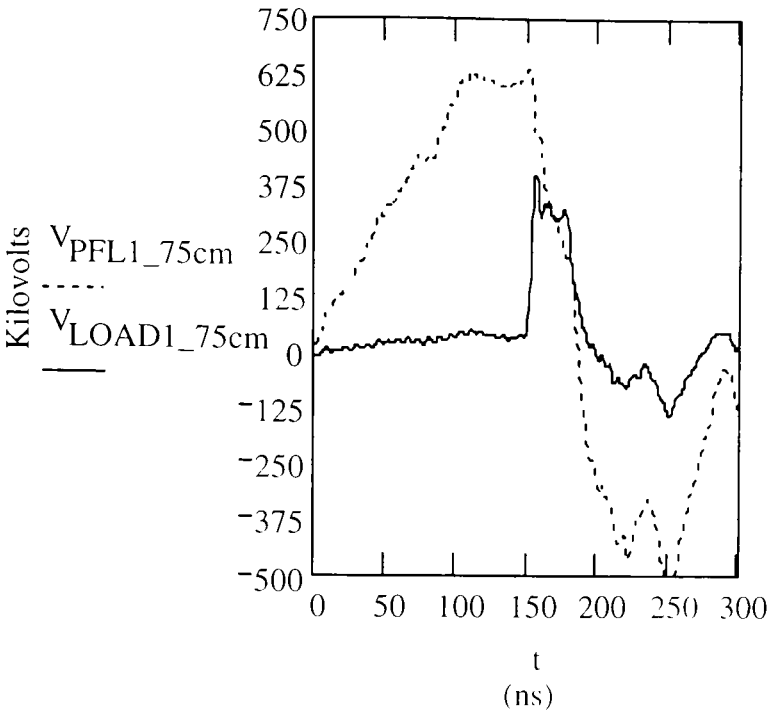

Figure 3.7. PFL and Load voltage for 1.75 cm gap spacing

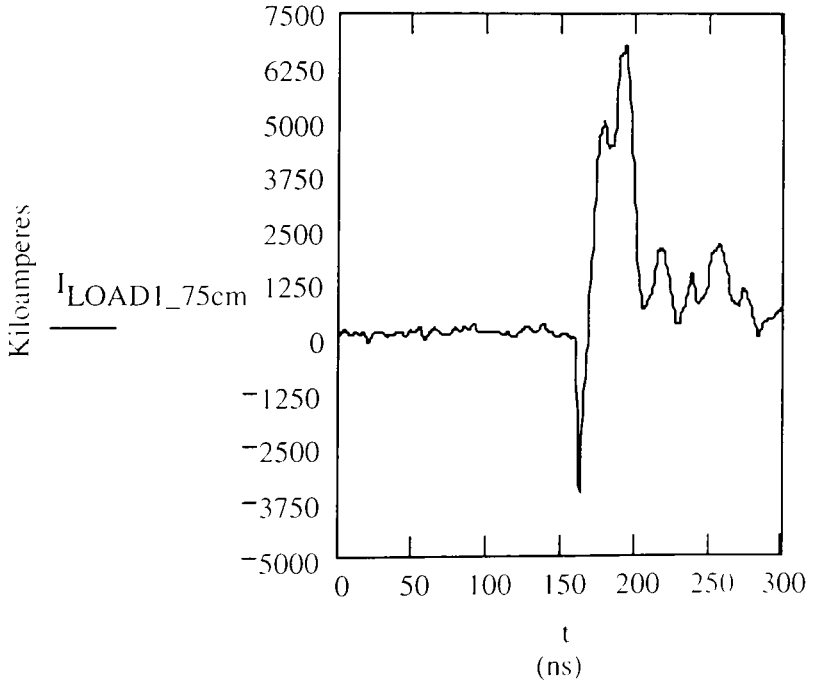

Figure 3.8. Beam current for 1.75 cm A-K spacing

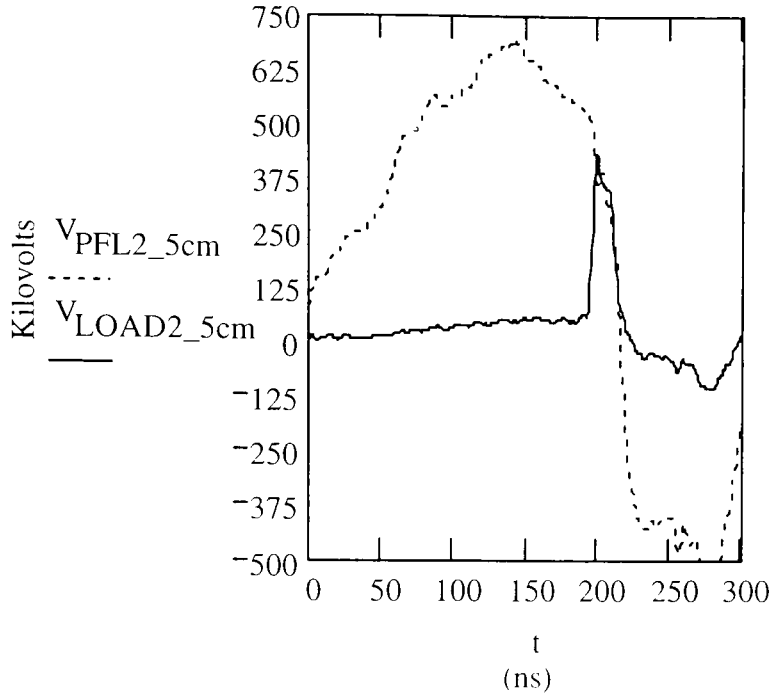

Figure 3.9. PFL and Load voltage for 2.5 cm A-K spacing

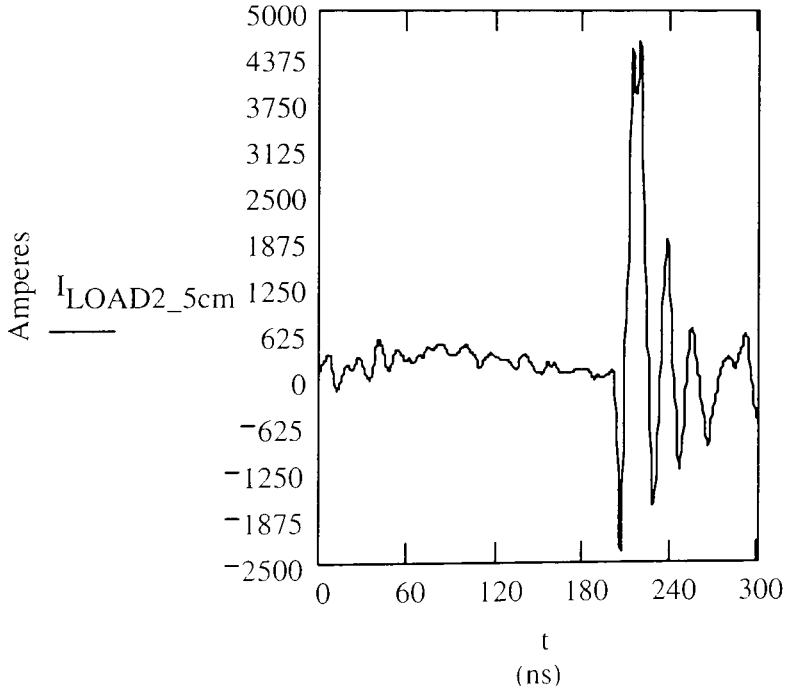

Figure 3.10. Beam current for 2.5 cm gap spacing

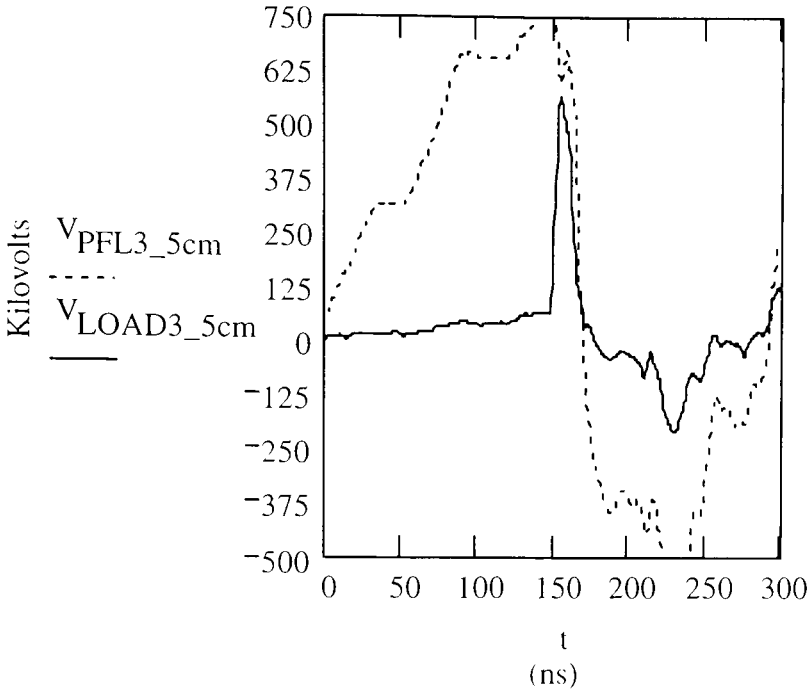

Figure 3.11. PFL and load voltage for 3.5 cm A-K spacing

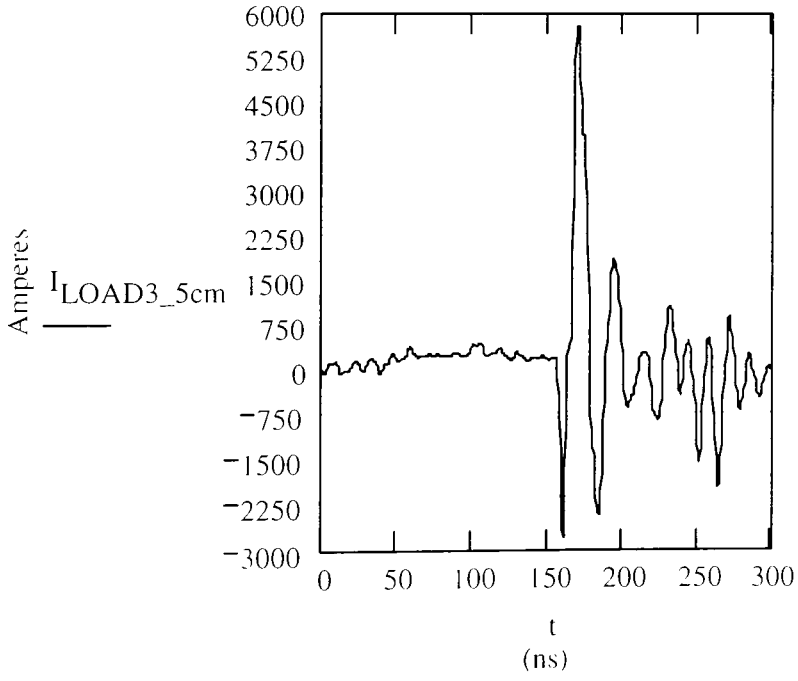

Figure 3.12. Beam current for 3.5 cm A-K spacing

Figures 3.5 through 3.12 display the voltage and current waveforms for 1, 1.5, 1.75, 2.5, and 3.5 cm Anode to Cathode (A-K) spacing. This data provides information on the input power and impedance of the diode (Table 3.1 and Figure 3.13, respectively), but shows an inconsistency between the 2.5 and 3.5cm, and the other three shots.

All of the shots display the same basic characteristic charging of the PFL at primary voltages of 50-53kV. The 150ns charging of the line is divided by characteristic "knees" at 60ns intervals. This is most likely the slow wave output of the Marx generator seeing an open circuit at the peaking gap until the line charges to the breakdown voltage, at which point for the 1-1.75cm shots, the switch closes, and a 60 ns 350-400kV output is delivered to the load. However, for the 2.5 and 3.5cm data sets, a shorter pulse is seen occurring as the switch breaks down several nanoseconds after the line reaches its peak voltage. Unfortunately this is due to the insulator failure that occurred at the Marx side of the PFL. Although these waveforms are not ideal cases, they still provided the necessary conditions for microwave generation, and therefore complete the comparison for the range of A-K spacing.

Figure 3.13 displays a comparison of measured values for diode impedance in comparison with values calculated using a fixed diode voltage of 400 kV divided by the Child-Langmuir current I_{CL} [8].

$$I_{CL} = 8.5 \cdot \left(\frac{r_m^2}{d^2} \right) \cdot \left(\sqrt{\gamma_o} - .8471 \right)^2$$

$$r_m := r_c + 0.7 \cdot d$$

where r_m accounts for beam flaring, with r_c as the cathode radius in cm (3cm), and γ_o is the relativistic factor:

$$\gamma_o := \frac{V_{diode}}{.511} + 1$$

Table 3.1. Diode Input Power

A-K spacing	1 cm	1.5 cm	1.75 cm	2.5 cm	3.5 cm
Diode Input Power (GW)	1.4	1.5	2	1.8	1.6

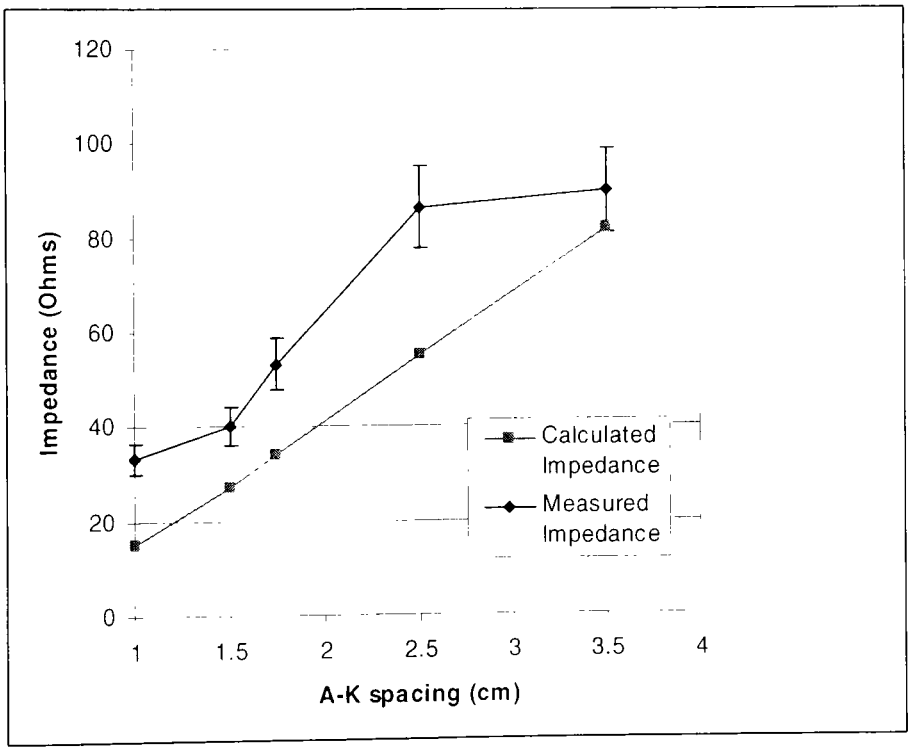

Figure 3.13 Diode Impedance versus A-K spacing

3.2 Microwave Generation

The principle of the Vircator is based upon the conversion of the kinetic energy of the electron beam into microwave energy. The oscillation of the charge between the Virtual Cathode and the real cathode, along with the movement of the Virtual Cathode itself contribute to the microwave generation.[6] Because of this, the frequency of the emitted microwaves is directly dependent upon the distance between the Anode and Cathode.

Figure 26 is the raw waveform recorded on the *Tektronix* 6Ghz digital oscilloscope for the June 5th 1.5cm shot. As mentioned in the beginning of section 3.1, some of the RF data taken on this day was clipped. Because of this, the 1.5cm shot is used to obtain a factor relating the power calculated from the b-dot signal, to the power contained in the microwave envelope of the Balun/detector. This allows for a rough idea of power output for the other two shots.

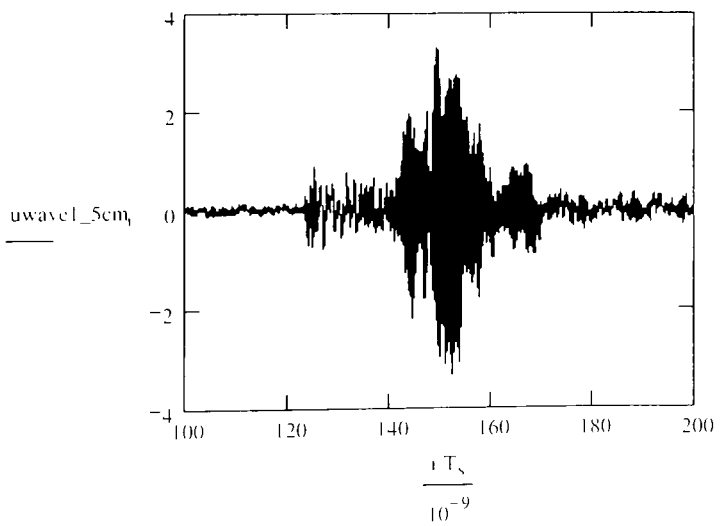

Figure 3.14. B-dot RF waveform for 1.5 cm A-K spacing

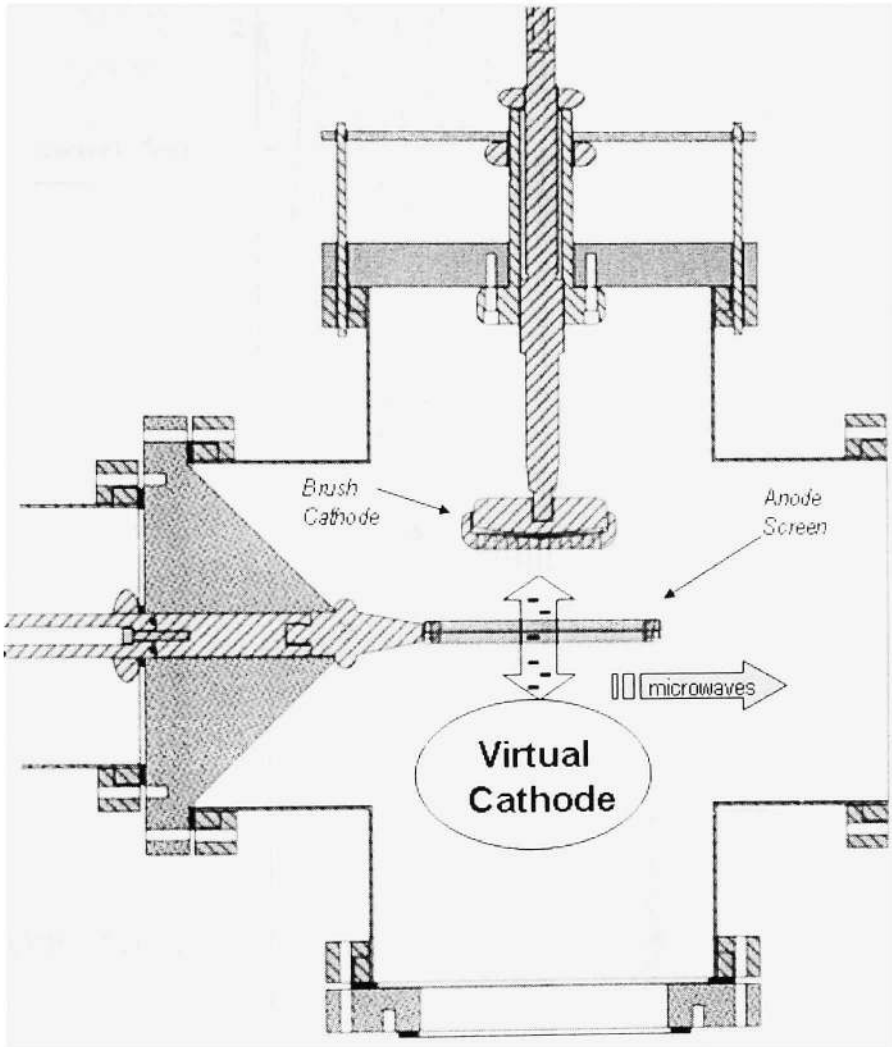

Figure 3.15. Detail of the Reflex Triode Vircator

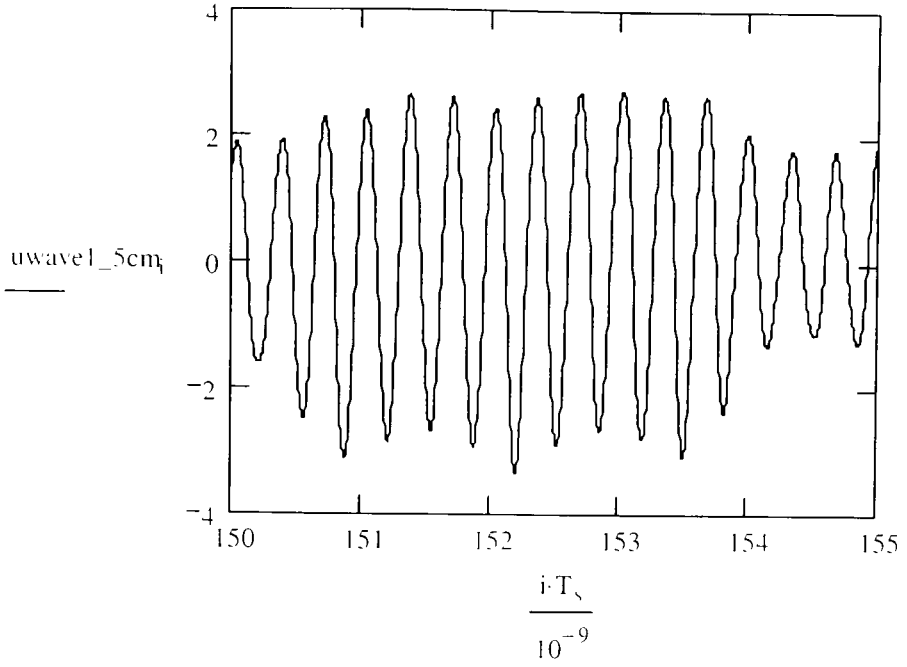

Figure 3.16. Zoomed microwave data for 1.5 cm A-K spacing

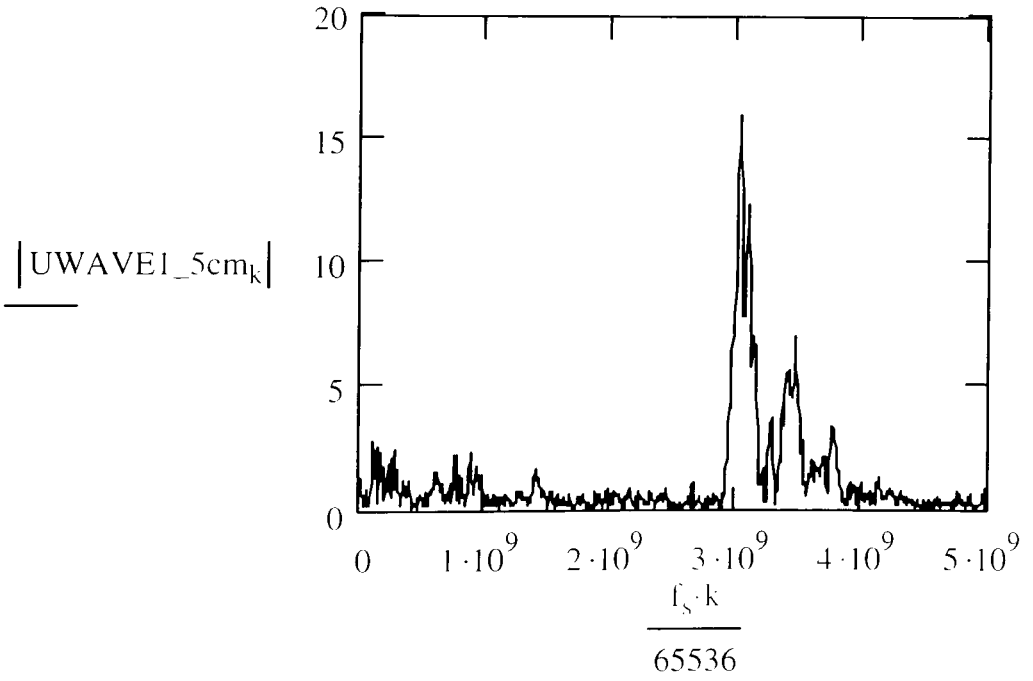

Figure 3.17. FFT of B-dot waveform for 1.5 cm A-K spacing

The actual *MathCAD* worksheet for analysis of the RF data is contained in the Appendix of this thesis[10]. In the worksheet the Fast Fourier Transform (FFT) of the microwave data in Figure 26 is taken to determine the frequency for the shot (Figure 29). Taking into account the equivalent area and inductance of the probe, and the attenuation from the diagnostics, the magnetic field B is calculated for the loop (Figure 30).

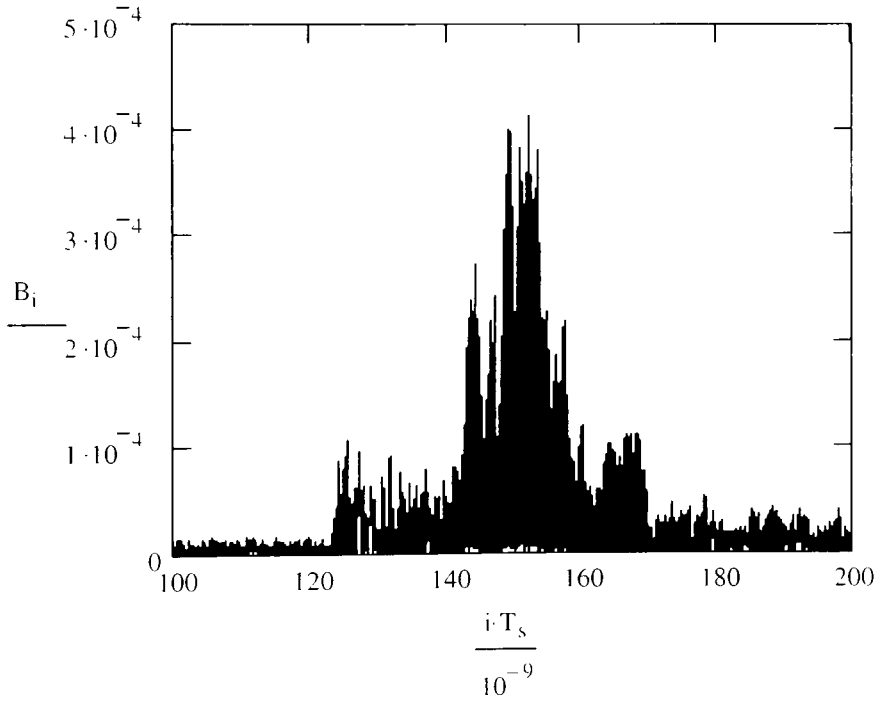

Figure 3.18. Magnetic field from B-dot

From this, the magnetic flux density is calculated.

$$S_i := \left(B_i\right)^2 \cdot \frac{c}{\mu_0}$$

Using this data and calculating the beam width for the given probe distance (45 inches), the peak power is determined (Figure 3.19).

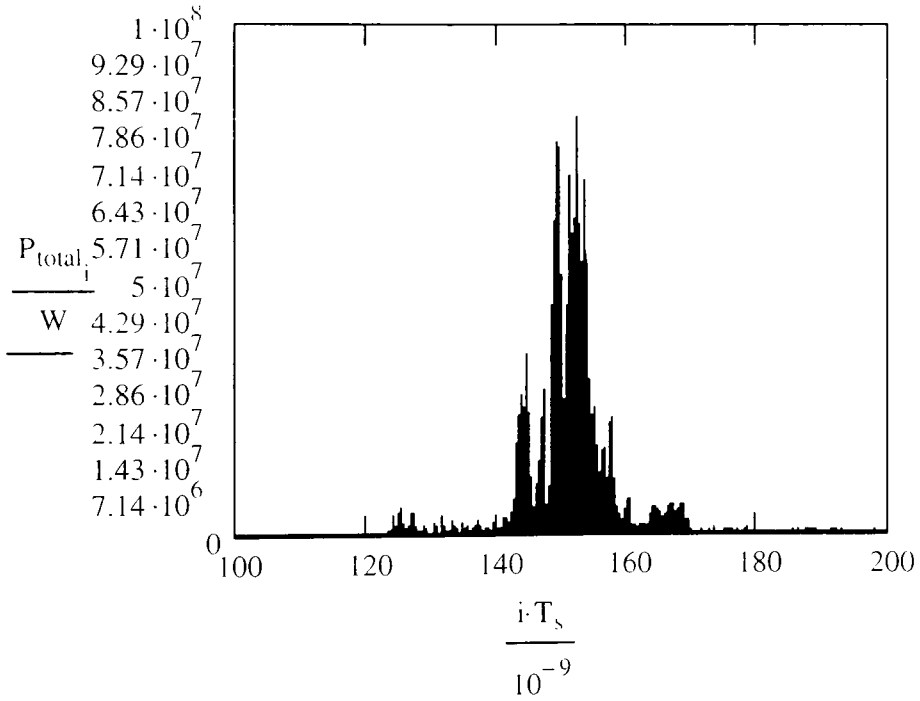

Figure 3.19. Total emitted microwave power for 1.5 cm A-K spacing

Again, the above information is used as a basis of comparison for the other microwave data. Knowing that the waveform recorded from the Balun/detector is nothing more than the envelope of the RF signal, the power level from Figure 31 is compared to the envelope for the same shot (Figure 3.20).

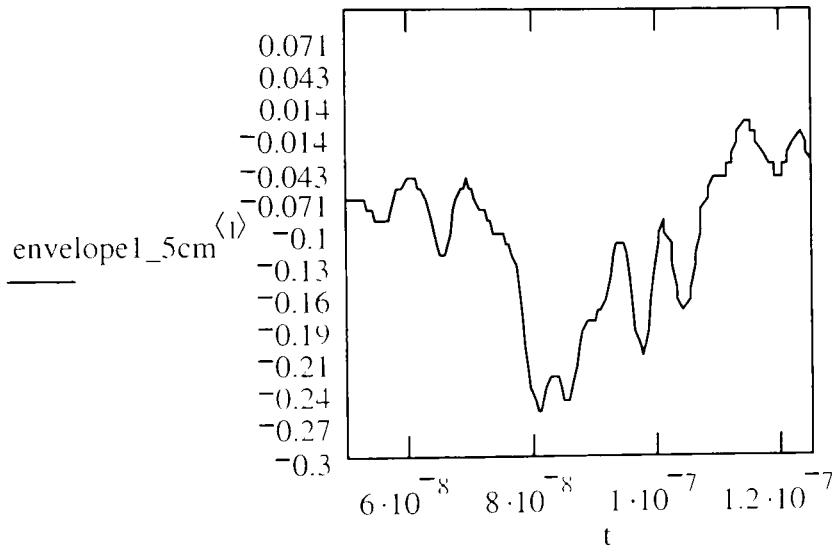

Figure 3.20. Envelope signal from Balun/detector for 1.5 cm A-K spacing

The maximum RF power is divided by the scope voltage, obtaining the factor K_{RF_env}.

$$V_{max\_env} := -.26 \cdot V$$

$$P_{max\_RF} := 80 \cdot 10^{6}\ W$$

$$K_{RF\_env} := \frac{P_{max\_RF}}{V_{max\_env}}$$

$$K_{RF\_env} = -3.077 \times 10^{8}\ A$$

Multiplying this factor by the y-axis values for the envelope, an approximate value for power is calculated for the envelope data (Figure 3.21).

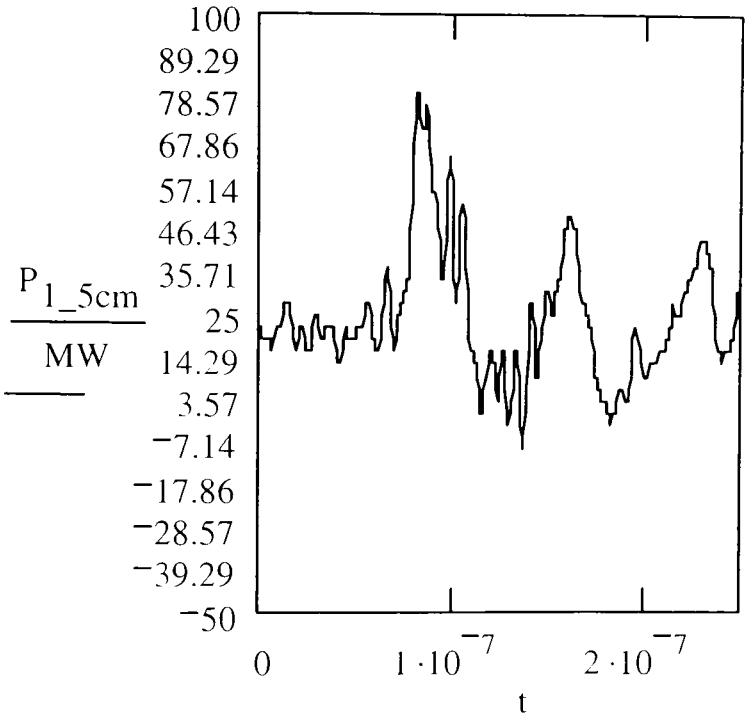

Figure 3.21 Microwave power from Balun/Detector data for 1.5 cm A-K spacing

The waveforms for 1 and 1.25 were considerably stronger signals (hence the clipping) because of a weak firing of the pulser on the 1.5 cm shot, and because of a noticeable decrease in microwave power for Anode-Cathode spacing at or above 1.5cm. Figure 34and 36 are the scope waveforms for the 1 and 1.25 cm shots respectively. Also, pictured in Figures 3.23 and 3.24 are the same signals multiplied by K_{RF_env}. Although these are not completely accurate representations of microwave power, they do give an idea of the order of magnitude for microwaves generated by the Reflex Triode Vircator.

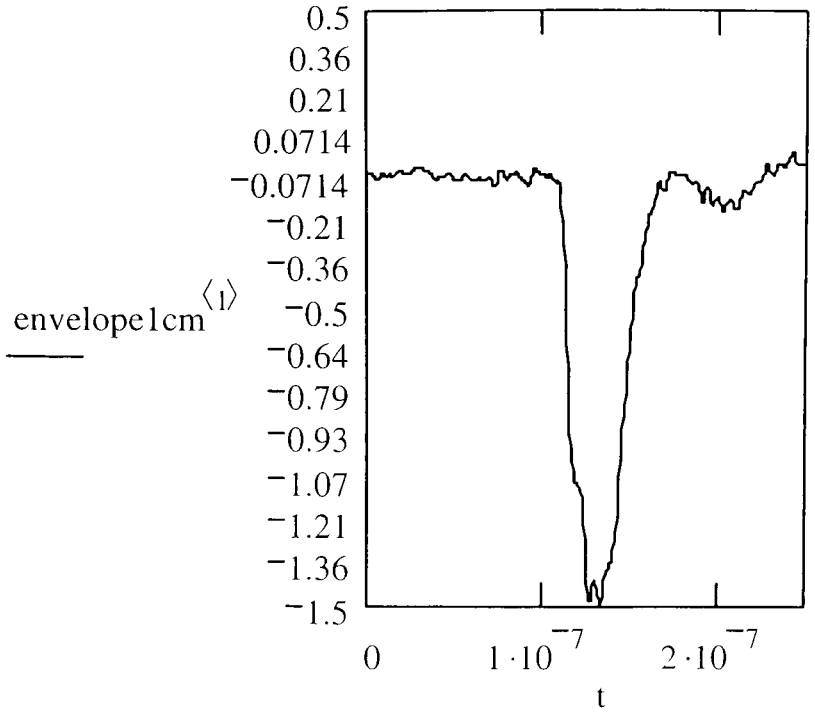

Figure 3.23. Raw scope data from Balun/detector for 1 cm A-K spacing

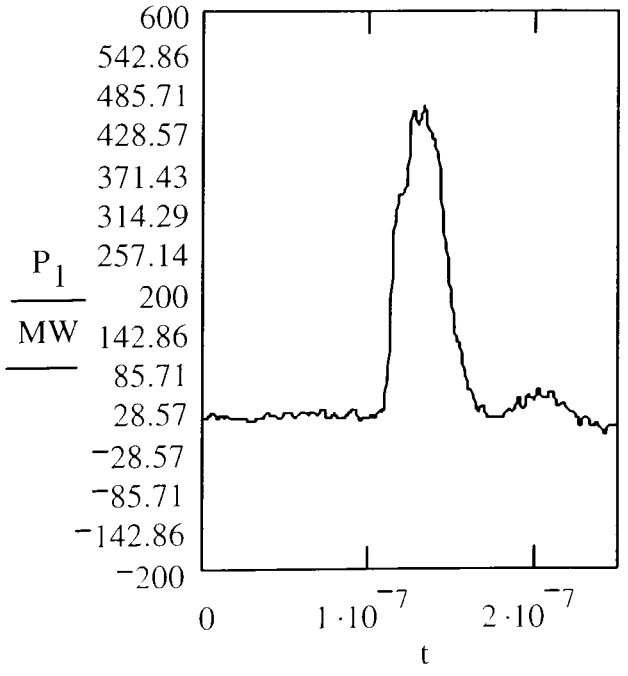

Figure 3.24. Approximated microwave power for 1 cm A-K spacing

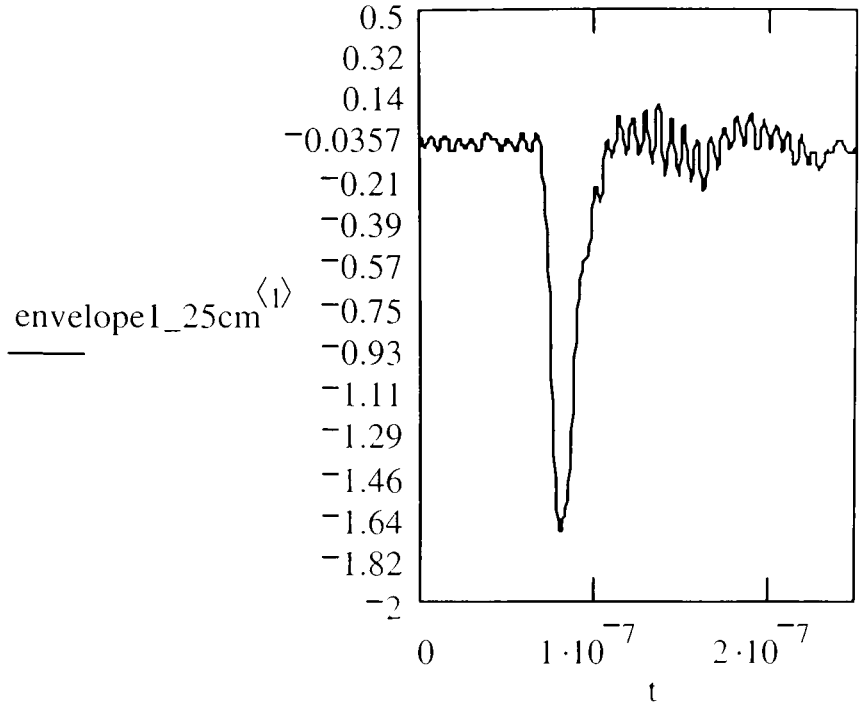

Figure 3.25. Raw scope data from Balun/detector for 1.25 cm A-K spacing

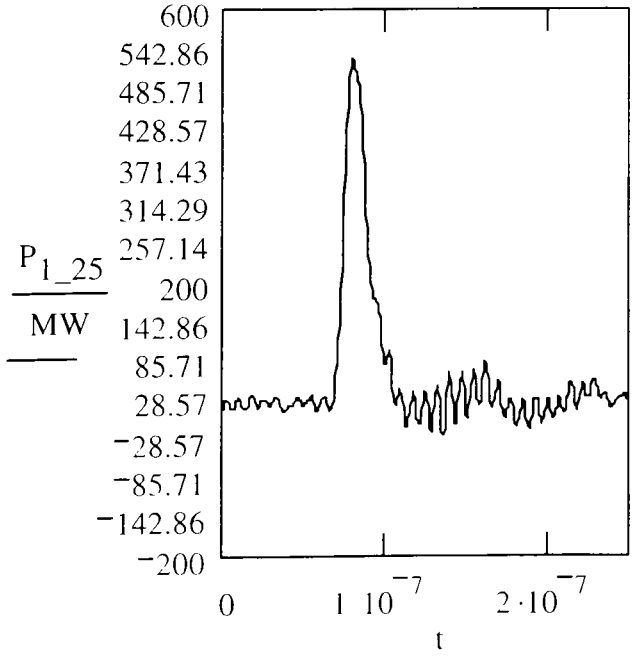

Figure 3.26. Approximated microwave power for 1.25 cm A-K spacing

As stated at the beginning of this section, the A-K spacing directly affects the frequency of the microwaves generated by the Virtual cathode. Figures 3.26-3.28 plot the FFT spectrum for 1, 1.25, and 1.5cm gap distances. The main peak is seen shifting almost a full GHz for every .25cm of change in the diode gap.

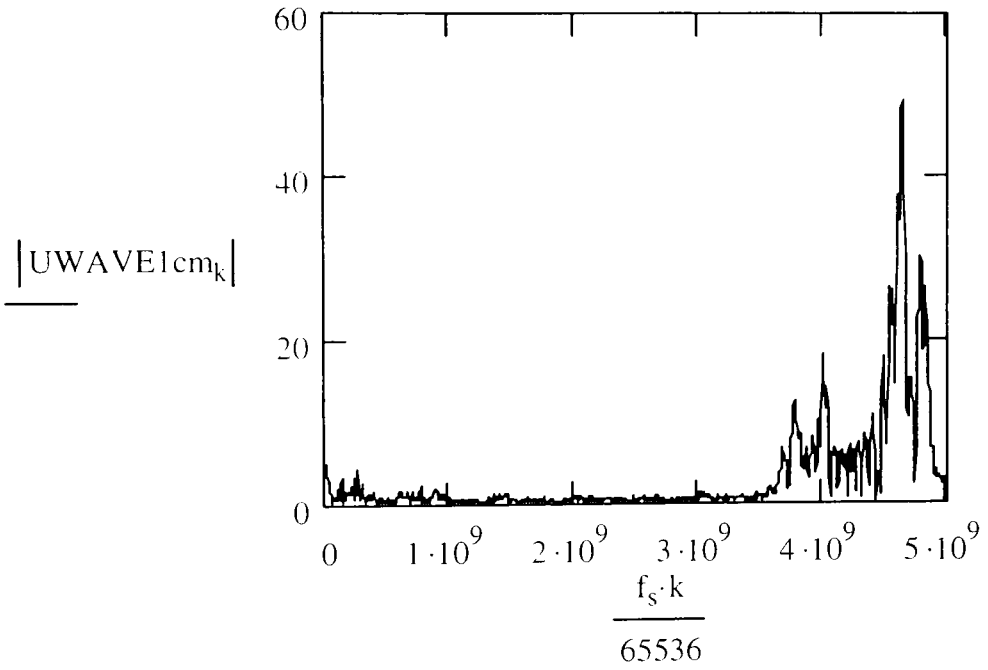

Figure 3.27. Frequency spectrum for 1cm A-K spacing

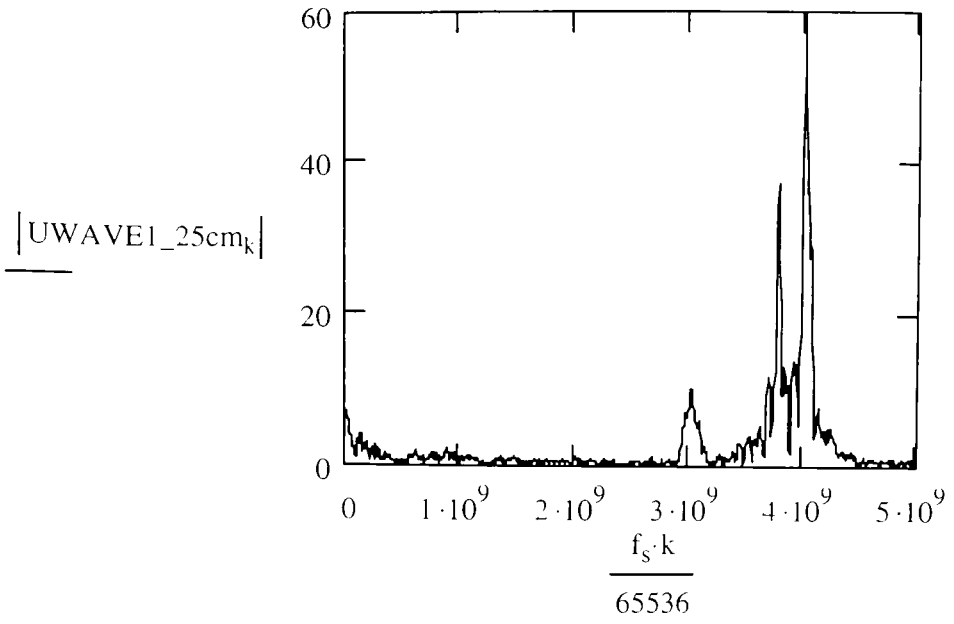

Figure 3.28. Frequency spectrum for 1.25 cm A-K spacing

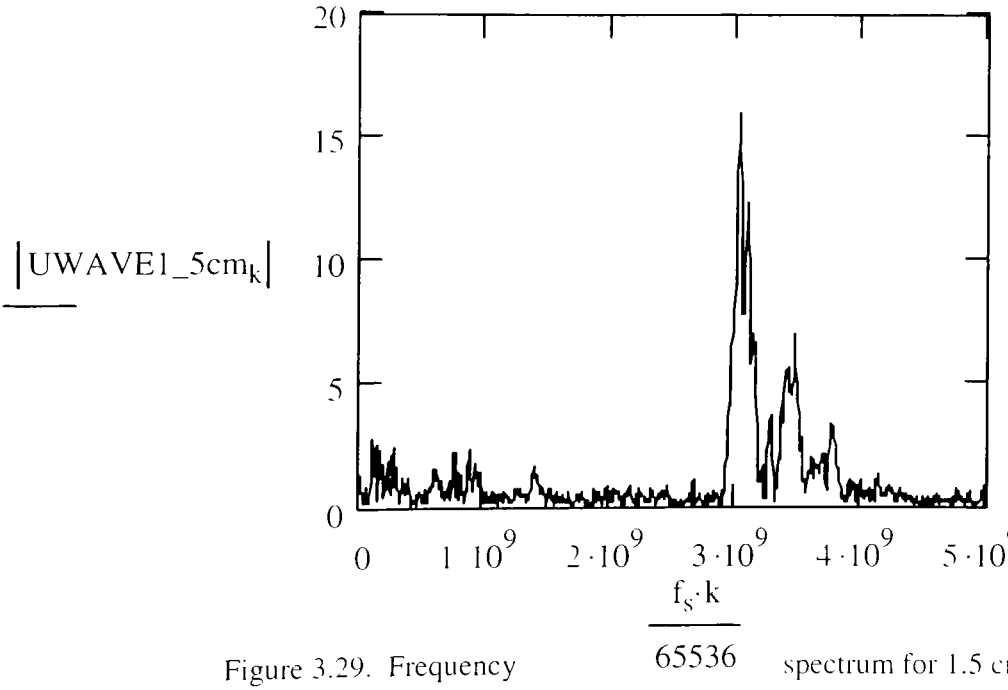

Figure 3.29. Frequency spectrum for 1.5 cm A-K spacing

CHAPTER IV

CONCLUSIONS AND SUGGESTIONS FOR FUTURE WORK

Although the project found its end in the temporary demise of the pulser, the test bed is a functional and stable platform for studying high-power microwaves. Changing the transmission line supports/feed-throughs to simple, non-sealing supports increased the lifespan of the machine considerably by eliminating discontinuities in the dielectric composition of the transmission line, and consequently diminishing the chance of internal breakdown at higher voltage levels. This coupled with the already large aspect ratios and size, make for a very robust system.

At the conclusion of the project, the diagnostics were tuned, calibrated, and shielded from external noise. The capacitive probes, although somewhat difficult to accurately calibrate, were reliable and simple to construct.

The B-dots and Baluns used are the subject of a paper by Dr. John Mankowski written at the same time as the Thesis [10], and will allow any future work in this subject to have a documented and calibrated detector. If similar studies are done, these detectors could be used in an array to determine field patterns, mode, and power levels.

The Reflex Triode utilizing the brush cathode as an emission source is a hotly contested subject due to the inordinately high claims of efficiency (%40) by its original innovators, *Didenko et. al.* The data taken on this project neither substantiates, nor refutes this claim, as the efficiencies ranged from 8% to 15%. Using the existing set-up, and

continuing where this document concludes could easily yield very complete results pertaining to the feasibility of the Triode.

To gain a more complete understanding of the brush cathode as an emission source, several devices may be employed. The Acetate film is an excellent visual diagnostic for seeing the pattern and intensity of the e-beam. Using a smaller radius cathode to reduce the chances of breaking down to the anode screen, a comparison can be made between the metal pin and velvet as field emission devices.

REFERENCES

[1] A.N. Didenko, A.G. Zherlitsyn, A.S. Sulakshin, G.P Fomenko, V.I. Tsetkov, and Yu. G. Shteyn, "The Generation of High-Power Microwave Radiation in a Triode System by a Heavy-Current beam of Microsecond Duration", Sov. Tech. Phys. Lett., Vol. 4, 1978 p.3

[2] D. Lojevski, dissertation "Experimental Investigations of Water Breakdown," Texas Tech University (1996)

[3] S.T. Pai and Q. Zhang, "Introduction to High Power Pulse Technology", River Edge NJ, World Scientific Publishing Co., 1995

[4] Tammo Heeren, *MathCAD* worksheet for the construction of a copper-sulfate water resistor, 2001

[5] Dr. James Dickens, Texas Tech University, Personal Communication, 2003

[6] J. Benford and J. Swegle, "High-Power Microwaves," MA : Artechhouse, Inc., 1992

[7] K. Woolverton, "High Power, Coaxial Vircator Geometries," Texas Tech University, (1998)

[8] D. Cheng, "Field and Wave Electromagnetics," MA: Addison-Wesley Publishing, 1989

[9] S. Calico, "High-Power Microwave Breakdown of Dielectric Interfaces," Texas Tech University, 1991

[10] Dr. John Mankowski, Paper, "A B-dot Sensor and Balun Assembly for Detection of Pulsed Power Microwaves," 2003

APPENDIX

The addition of a resonant cavity was to be used as part of this work, and should be utilized in any future research. Figures 4.1 and 4.2 show *Ansoft HFSS* information for the E-fields of a 4.5" diameter by 4.5" length cavity stimulated internally with a 2GHz source. The 1.6" diameter extraction aperture showed the highest external field while maintaining the Q of the cavity.

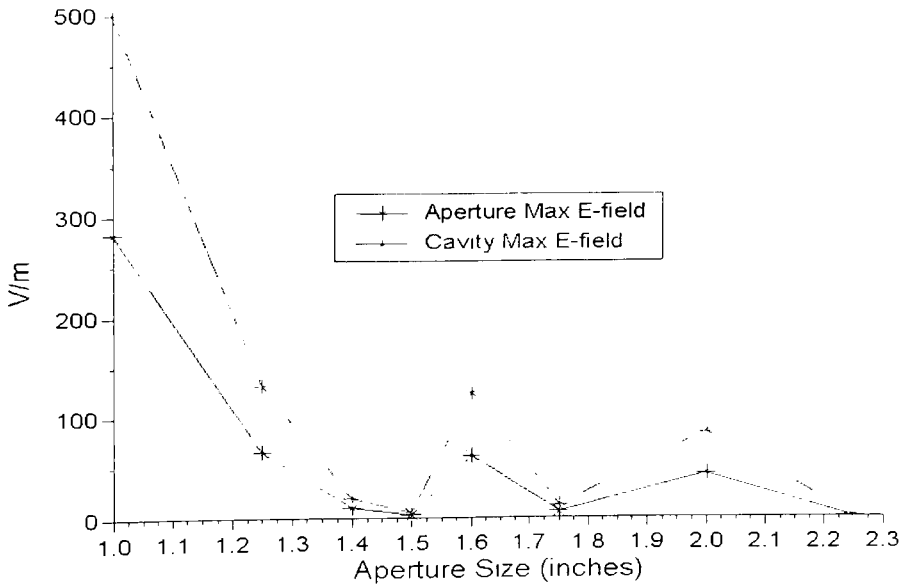

Figure 4.1. Relative E-field for aperture vs. cavity

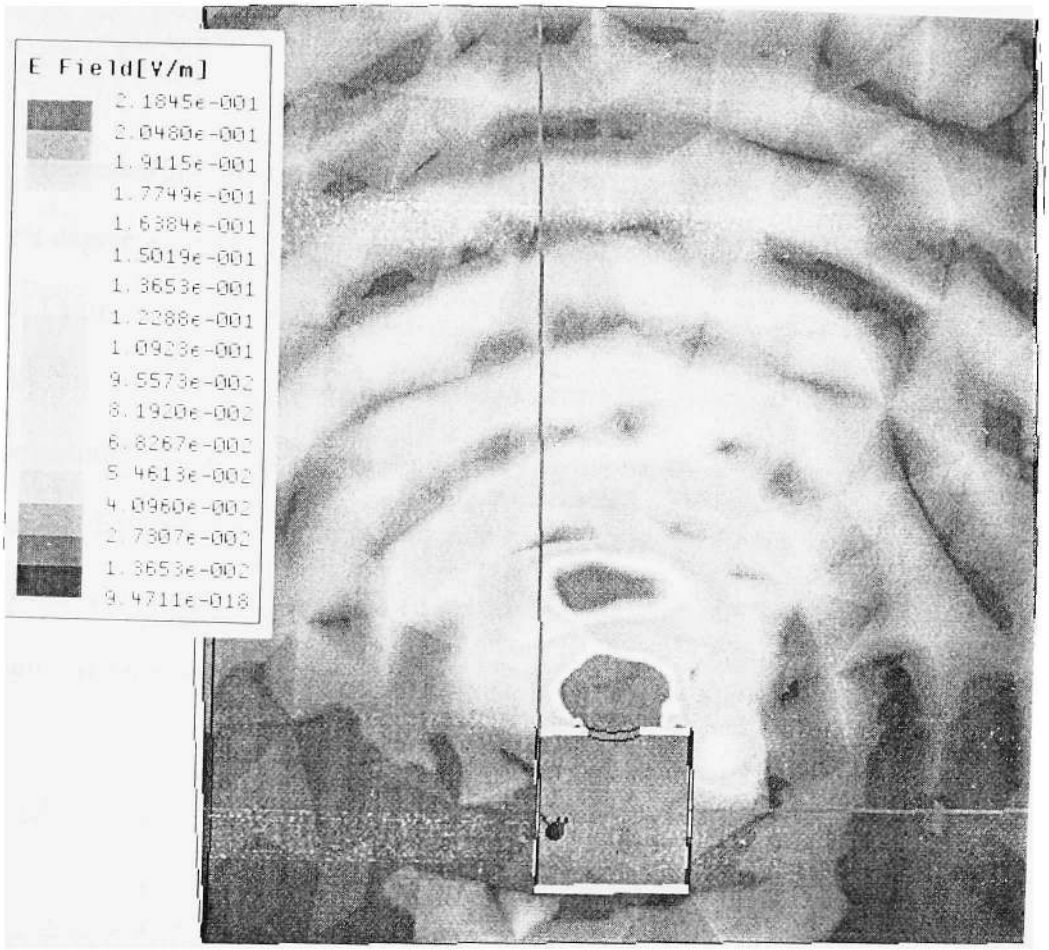

Figure 4.2 External E-field from cavity

PERMISSION TO COPY

In presenting this thesis in partial fulfillment of the requirements for a master's degree at Texas Tech University or Texas Tech University Health Sciences Center, I agree that the Library and my major department shall make it freely available for research purposes. Permission to copy this thesis for scholarly purposes may be granted by the Director of the Library or my major professor. It is understood that any copying or publication of this thesis for financial gain shall not be allowed without my further written permission and that any user may be liable for copyright infringement.

Agree (Permission is granted.)

Student Signature _____ Date _____

Disagree (Permission is not granted.)

_____ _____

Student Signature Date